Title	Investigating the mechanical properties of GeSn nanowires.
Authors	Kosmaca, Jelena;Meija, Raimonds;Antsov, Mikk;Kunakova, Gunta;Sonders, Raitis;Iatsunskyi, Igor;Coy, Emerson;Doherty, Jessica;Biswas, Subhajit;Holmes, Justin D.;Erts, Donats
Publication date	2019-07-10
Original Citation	Kosmaca, J., Meija, R., Antsov, M., Kunakova, G., Sondors, R., Iatsunskyi, I., Coy, E., Doherty, J., Biswas, S., Holmes, J. D. and Erts, D. (2019) 'Investigating the mechanical properties of GeSn nanowires', Nanoscale, 11(28), pp. 13612-13619. doi: 10.1039/c9nr02740h
Type of publication	Article (peer-reviewed)
Link to publisher's version	https://pubs.rsc.org/en/content/articlelanding/2019/nr/c9nr02740h#!divAbstract - 10.1039/c9nr02740h
Rights	© The Royal Society of Chemistry 2019
Download date	2025-02-12 16:50:35
Item downloaded from	https://hdl.handle.net/10468/8214

Investigating the Mechanical Properties of GeSn Nanowires

Jelena Kosmaca,[a] Raimonds Meija,[a] Mikk Antsov,[a] Gunta Kunakova,[a] Raitis Sondors,[a] Igor Iatsunskyi,[b] Emerson Coy,[b] Jessica Doherty,[c,d] Subhajit Biswas,[c,d] Justin D. Holmes[c,d] and Donats Erts[a,e *]

[a]*Institute of Chemical Physics, University of Latvia, 1 Jelgavas str., Riga, LV-1004, Latvia*

[b]*NanoBioMedical Centre, Adam Mickiewicz University, 85 Umultowska str., Poznan, PL 61614, Poland*

[c]*School of Chemistry, ERI and the Tyndall National Institute, University College Cork, Cork, T12 YN60, Ireland*

[d]*AMBER@CRANN, Trinity College Dublin, Dublin 2, Ireland.*

[e]*Faculty of Chemistry, University of Latvia, 1 Jelgavas str., Riga, LV-1004, Riga, Latvia*

*Corresponding author, email: donats.erts@lu.lv, address: University of Latvia, 19 Raina blvd., Riga, LV-1586, Latvia

Abstract

Germanium tin (GeSn) has been proposed as a promising material for electronic and optical applications due to the formation of a direct band-gap at a Sn content >7 at.% and its compatibility with Si. Furthermore, the ability to manipulate the properties of GeSn at the nanoscale will further permit the realisation of advanced mechanical devices. Here we report for the first time the mechanical properties of Ge_{1-x} Sn_x nanowires (7.1 – 9.7 at % Sn) and assess their suitability as nanoelectromechanical (NEM) switches . Electron microscopy analysis showed the nanowires to be single crystalline, with surfaces covered by a thin native amorphous oxide layer. Mechanical resonance and bending tests at different boundary conditions were used to obtain size-dependent Young's moduli and to relate the mechanical characteristics of the alloy nanowires to nanowire geometry and Sn incorporation. The mechanical properties of the GeSn alloy nanowires make them highly promising for applications in next generation NEM devices.

Keywords

Germanium tin alloy, nanowire, size dependence, mechanical behaviour

Introduction

Direct band-gap group IV semiconductors, such as Ge or Si, can be formed by alloying with elements such as Sn and Pb, [1,2] leading to numerous applications such as efficient band-to-band tunnelling devices, *e.g.* tunnelling field effect transistors, [3,4] lasing platforms [5,6] and mid-infrared photonic devices, *e.g.* waveguide amplifiers. [7] Group IV alloys are compatible with current Si processing technology, an advantage over III-V materials, and recently there have been a number of reports on utilising GeSn and SiGeSn in films in electronic, [8,9] optoelectronic [10,11] and photonic [6,12–14] devices.

However, the lattice mismatch between Ge, Sn and Si in thin films causes significant strain within thin films. One solution to overcome strain in group IV alloys, such as GeSn, is to produce one dimensional nanostructures; nanowires allow for increased strain relaxation compared to thin films due to free sidewall facets. [15] Recently, the growth of GeSn nanowires has been achieved by top down [16–19] and bottom up approaches, [20–25] including the bottom up grown Ge/GeSn core/shell nanowires. [15,20,26] GeSn nanowires (with > 7 at. % Sn) have also been reported to display a direct bandgap [20] photoluminescence. We have previously reported the growth of direct band-gap GeSn nanowires using a three phase vapour-liquid-solid (VLS) process, resulting in uniform nanowires with a high Sn loading (≈ 9 at. %) and good crystal quality. [21,23]

GeSn nanowires are also promising candidates for nanoelectromechanical and nanooptoelectromechanical systems. [27] We have previously reported the exceptional mechanical strength of Ge nanowires, with radii between 20 to 80 nm [28] and have utilised these nanowires to form voltage-controlled, two-terminal bistable NEM devices. [29–31] Young's modulus is a decisive property for the application of nanowires as NEM switching devices, as it defines the device operation parameters, such as speed and voltage, as well as influencing contact reliability and the lifetime of a device. [32] Previously reported Young's moduli of crystalline Ge nanowires were derived from bending [28] and resonance [33] measurements; the values obtained were comparable to bulk Ge material and did not exhibit size-dependence at radii below 100 nm.

To the best of our knowledge, there have been no reports to-date on the mechanical properties of GeSn alloy nanowire. However, the amount of Sn in GeSn can potentially influence the

mechanical behaviour of the alloy. [34] A theoretical Young's modulus of 82 GPa extracted from ab initio calculations for GeSn material with 50% atomic percentage of Sn [35] suggests that Sn may cause softening of the material, as has been observed for Ti-Nb-Sn alloy samples at higher Sn concentrations. [34]

The intrinsic mechanical properties of a material at the nanoscale may also significantly differ from that of the bulk material. Commonly observed size-dependent mechanical properties at the nanoscale are influenced by factors such as crystalline structure [36] and defects. [37] These size effects are expected to become more prominent as dimensions are reduced to the nanoscale. [36] However, size dependence of the mechanical properties have been observed also for nanowires with diameters comparable to 100 nm. [38] Commonly, size-dependent mechanical properties of crystalline nanowires are interpreted in terms of surface effects [39], which can be attributed to surface elasticity and surface stress. [40–42] One of the factors decisive for surface effect is the bonding type of material. For example, decrease of the Young's modulus with decreasing diameter, i.e. softening effect, has been previously reported for Si nanowires with covalent bonds. [39,43] In the case of GeSn, which has a similar diamond cubic structure as silicon, similar effect is expected. Nanowires can exhibit stiffening, softening or no size effect under different loading modes (e.g. dynamic resonance, static bending or tension) [44] and boundary conditions (e.g. single- or double-clamped) due to surface effects. [44–46] Typically observed nanowire morphological features, like tapering [37,47] and surface oxidation, [28,29,48] can also impact their mechanical performance, since even a thin oxide layer could affect the surface stress. For oxide thicknesses comparable with nanowire radii, a core-shell model can be used to explain the size-dependence. [38,41]

This article reports for the first time the mechanical properties of bottom-up synthesised GeSn nanowires, with up to 9 at.% Sn atoms distributed throughout the crystal structure of the nanowires. [23,49] The mechanical properties of the nanowires were assessed by various experimental approaches, such as mechanical resonance [37,38,51,52] and bending tests [28,33,53], which can be performed with either atomic force microscopy [28] or *in-situ* electron microscopy [31,50,51]. The mechanical properties of these novel nanowires were compared to previously reported properties of pure Ge nanowires. [28,33,50] The physical properties of the GeSn nanowires were analysed in the context of assessing their suitability for future NEM devices. [32]

Experimental

GeSn nanowires (with 7-9 at.% Sn inclusion) were synthesised by a liquid-injection chemical vapour deposition technique, where the growth of the nanowire follows the vapour-liquid-solid (VLS) paradigm. [21,23]

GeSn nanowires (with 7-9 at.% Sn inclusion) were synthesised by a liquid-injection chemical vapour deposition technique, as previously reported.[21] Dodecanethiol-stabilised Au nanoparticles were used as growth seeds, which were spin-coated onto a Si (001) substrate containing a native oxide. The substrate was loaded into a metal reaction vessel which was then left under vacuum at 180 °C overnight to ensure a moisture free growth atmosphere and the desorption of the surfactant molecules.

Solutions of diphenylgermane (DPG) and allyltributylstannane (ATBS) in anhydrous toluene were prepared in an N2 filled glove box with a typical Ge and Sn precursor concentration of 0.025 mL and 0.0075 mL respectively in 10 mL toluene. A solution containing both Ge and Sn precursors was loaded into a Hamilton sample-lock syringe inside the nitrogen-filled glovebox. Prior to injection, the coated Si substrate was further annealed for 15 min at 440 ºC

under a flowing H2/Ar atmosphere inside a tube furnace. The precursor solution was then injected into the metal reaction vessel using a high-pressure syringe pump at a rate of 0.025 mL min-1. A H_2/Ar flow rate of 0.6 sccm was maintained during the entire growth period. A typical nanowire growth time was 2 h.

The morphology and structure of the nanowires were assessed by scanning and transmission electron microscopy (SEM Hitachi S-4800, TEM JEOL ARM-200F Probe corrected). Prior to the resonance and bending measurements by *in-situ* SEM, individual GeSn nanowires were attached to sharp electrochemically etched Au tips using Smaract and Attocube nanomanipulation systems inside an SEM. To ensure rigid nanowire-tip contacts [31,54], the nanowires were clamped with Pt strips deposited by a focused e-beam technique (SEM-FIB Tecnai Lyra).

The clamped nanowire diameters were measured from SEM images with a diameter precision of $\Delta_d = 5$ nm and length of $\Delta_L = 0.1$ μm. Their mean radii were calculated as $r \pm \Delta_r = 0.5(r_0 + r_1) \pm 5$ nm, where $r_0 = 0.5d_0$ and $r_1 = 0.5d_1$, were measured at the clamped and free end. Nanowire tapering parameter $\sigma = (r_0 - r_1)/L$ was calculated to be less than 0.01, which corresponds to facet taper angles α of less than ~1.1°.

Nanowire resonance was excited by applying an oscillating electric AC/DC signal between the nanowire and electrode and detected visually by SEM. The excitation signal was powered by an AC sweep function generator (Agilent N9310A) and a DC voltage supply (Keithley 6487), monitored by an oscilloscope (TDS 1012). For each individual nanowire, resonance occurring at the first mode fundamental frequency was distinguished from the higher modes and parametric resonances by analysing nanowire vibration profiles and the

amplitude dependency on the AC and DC excitation signal amplitude. Resonance amplitude was determined from SEM images with an accuracy of 0.1 μm. The resonant frequency and quality factor *Q* were determined from Lorentzian fits of the acquired vibration amplitude-frequency plots.

The relative uncertainties of the experimental resonance Young's moduli r_E were estimated from the relative uncertainties for the experimentally measured nanowire diameter ($r_d = \Delta_d/d$), length ($r_L = \Delta_L/L$) and resonant frequency ($r_f \approx 1$ %) measurements, similarly to error analysis previously described in [55]. Relative uncertainty $r_E \approx 2r_f + 4r_L + 2(r_{d0} + r_{d1})$ resulted from classical Euler-Bernoulli beam theory formula for a cantilever, where $E \sim f^2 L^4 d^{-2}$. [56,57] The calculated r_E were in agreement with the bounds for the Young's moduli, calculated by finite element method (FEM) by varying modelling parameters of the nanowire geometry and frequency within their uncertainty range. Uncertainty from FEM data was assumed to be less than 1 % and had only had a minor contribution to r_E.

In the bending tests by *in-situ* SEM, the GeSn nanowires were bent using the edge of an atomic force microscope (AFM) chip. The deflection shape of the nanowires were determined from real-time SEM videos and images.

For the three point bending tests, the nanowires were mechanically transferred to a Ted-Pella AFM calibration grating. The sample surface was visualised by SEM to determine the appropriate configuration of the nanowires for performing the three point bend test. Further mechanical characterisation of individual suspended nanowires was conducted by atomic force microscopy (AFM) (Bruker Dimensions Edge). A number of force-displacement curves were taken for each measured nanowire and the mean Young's modulus and standard

deviation were calculated from the gradient of force-displacement plots. The Young's moduli calculated analytically were in agreement with the values obtained from FEM simulations (deviation less than 2%). The precision of the AFM was relatively high (XY and Z position sensor noise level is <0.5 nm and <0.2 nm, respectively) and compared to the uncertainties related to the actual measurements, can be neglected. There are a number of sources of error in the AFM three point bending measurements and they cannot be taken into account directly. Firstly, in each measurement, the AFM tip might not be in the same contact point as in the last measurement; as the tip is lifted between measurements and then lowered again to generate force-displacement curves. Secondly, thermal drift can affect the measurements resulting from different contact points on a nanowire with the AFM tip. Thirdly, during the measurement, as the force increases, the AFM tip might slip on top of the nanowire and again generate uncertainties. Those are the reasons, why the Young's modulus for each nanowire was measured several times, so that statistical analysis of the results could be performed.

Results and Discussion

Morphological Characterisation

GeSn nanowires with radii between 25-130 nm and lengths between 3-16 μm were selected for mechanical testing. From SEM measurements, the nanowires showed high length-to-radius aspect ratios of between 60-230, straight morphologies without any bend or kink and uniform circular cross-sections throughout the length of the nanowires (Figures 1(a) and (b)), as expected for AuAg-catalysed VLS grown GeSn nanowires. [23] The crystalline structure of the nanowires was confirmed by high resolution transmission electron microscopy (HRTEM) images. The amorphous shell (Figure 1(c)) was formed of Ge and Sn oxides. [58] Energy dispersive X-ray (EDX) analysis from different nanowires confirmed Sn inclusion between 7 to 9 at.% (Figure S1 in ESI). EDX analysis also confirmed the prevalence of oxygen in the

shells compared to the nanowire core, whilst Ge and Sn showed uniform radial and axial distributions (Figure 1(d)).

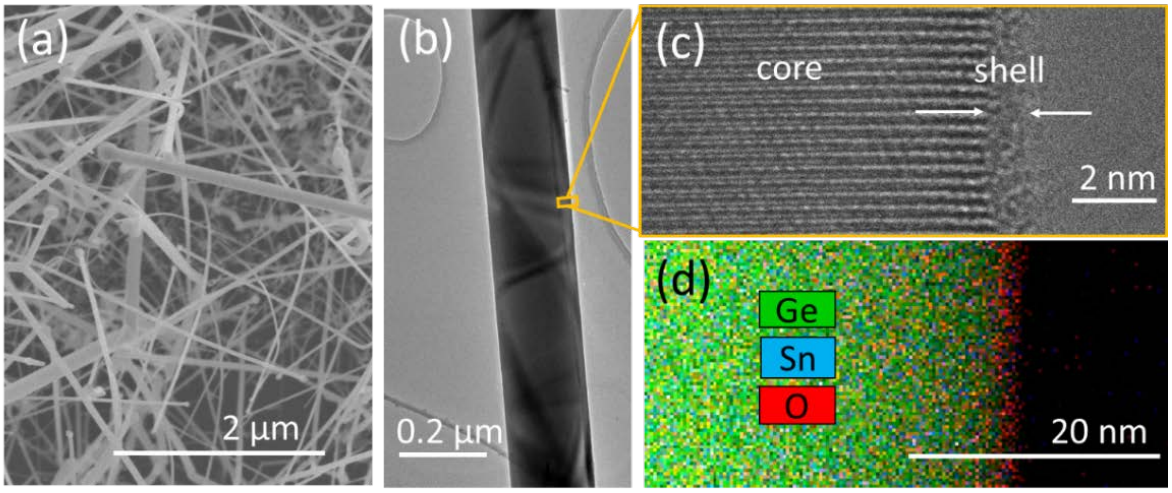

Figure 1: *(a) SEM image of GeSn nanowires grown on a Ge substrate; (b) TEM image of a GeSn nanowire with a radius* $r = 100$ *nm; (c) HRTEM image of a GeSn nanowire with a crystalline core and amorphous shell structure; (d) EDX elemental analysis mapping data of a nanowire core and shell.*

The observed shell thickness of between 1-2 nm (Figure 1(c)) on the GeSn nanowires was smaller than the previously reported thickness (2-7 nm) of the oxide shell previously observed on pure Ge nanowires [28,29] and could be assumed negligible compared to the core thickness of nanowires studied. Previous reports on Ge nanowires have emphasised the impact of oxidised surfaces on their electrical characteristics, [48] rather than on their mechanical properties. [28,33,50]

A proportion of the nanowires present on the substrate (Figure 1(a)) were found to be slightly tapered along their lengths. A small amount of tapering of long GeSn nanowires may result from competing diffusion-based mechanisms, where the radial growth is instigated by homoepitaxy and vapour-solid growth during the bottom-up VLS synthesis process. [23,49] One

thing to note is that the tapering in the GeSn nanowire was very minimal compared to conventionally tapered Ge nanowire. [59] HRTEM analysis also confirmed that there were no significant defects in the crystal structure of the GeSn nanowires synthesised (Figure 1(c)).

Mechanical Characterisation

The mechanical properties of GeSn nanowires were assessed by a combination of *in-situ* SEM resonance and bending tests of single-clamped nanowires (Figures 2(a) and (c)), and AFM three-point bending tests of nanowires suspended on trenches (Figures 3(a) and (b)). To extract information about Young's moduli and bending strengths of individual GeSn nanowires, experimentally obtained nanowire geometries, resonant frequencies and forces were simulated by the finite element method (FEM) (Figures 2(d), 3(c) and 3(d)).

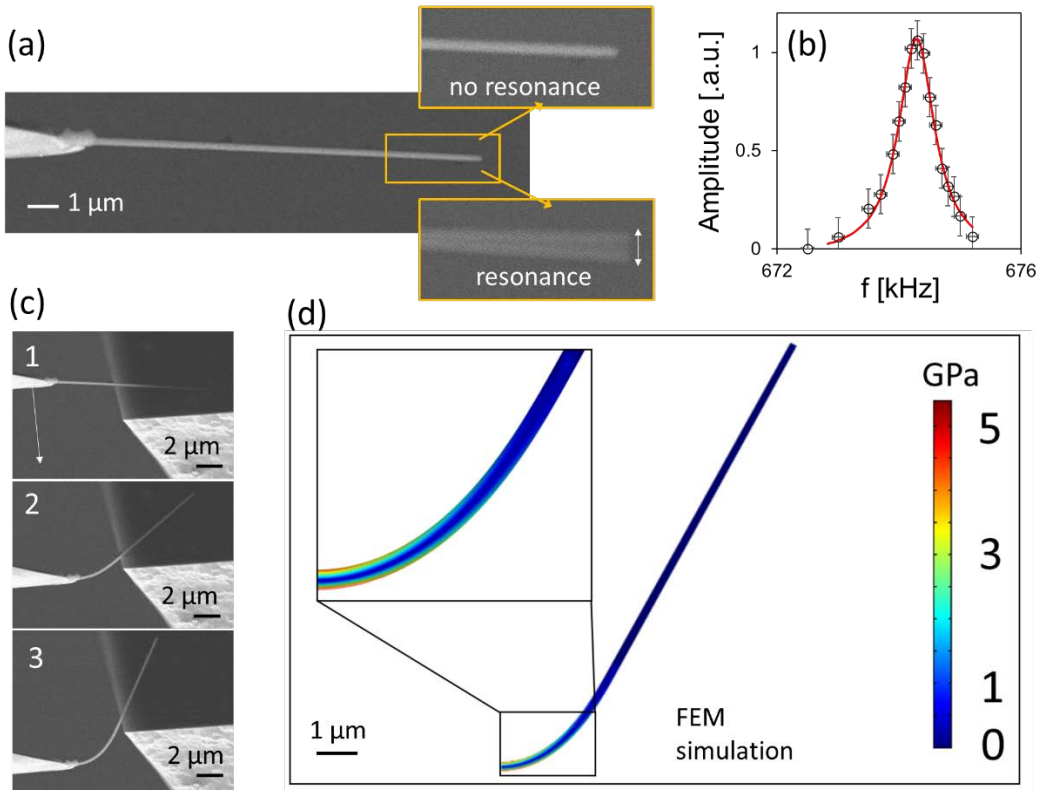

Figure 2: *(a) SEM image of a single-clamped GeSn nanowire; insets show nanowire end shape captured at a frequency far from and near resonance (white arrow indicating the vibration amplitude is added for clarity); (b) nanowire vibration amplitude measured near resonance and its Lorentzian fit (solid line); (c) Sequential (1→2→3) in-situ SEM images illustrating the GeSn nanowire shape during the bending process (indicative white arrow shows the direction of tip movement); (d) example of a FEM simulation of the stress distribution in the nanowire (for the shape on c3), used for determination of nanowire bending strength.*

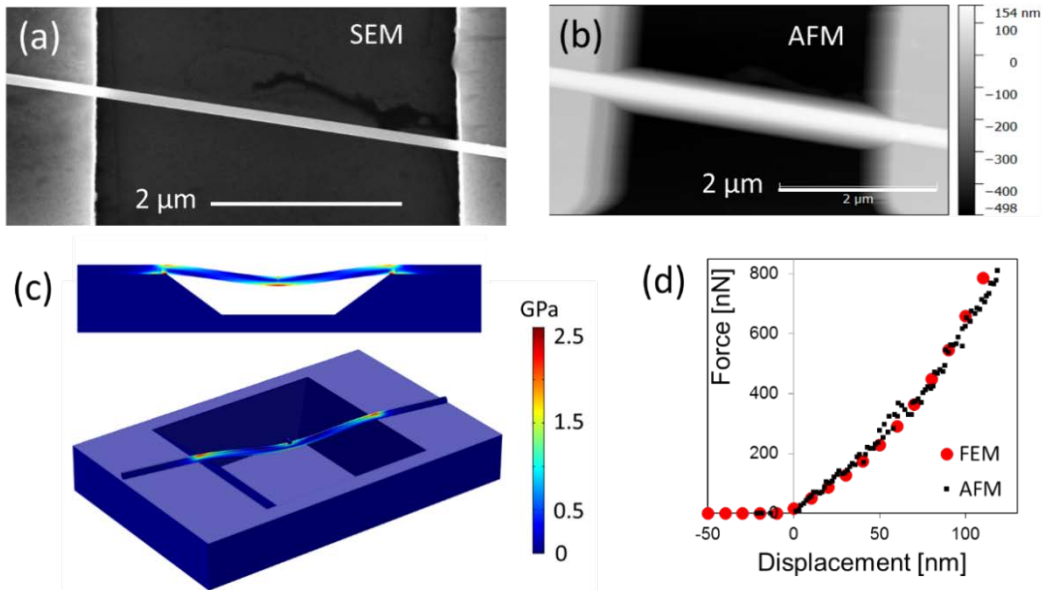

Figure 3: *(a) SEM and (b) AFM images for a GeSn nanowire suspended on a trench for three-point bending tests (top view); (c) FEM simulation of the bending test (cut plane through centre axis of the nanowire and three-dimensional model); (d) Force-displacement curves obtained during nanowire bending (black dots) and from FEM simulation (red circles), used for determining nanowire Young's modulus of the nanowire.*

Figure 2(a) illustrates a SEM image of the first mode mechanical resonance for a typical single-clamped GeSn nanowire with length $L = 15\ \mu m$ and mean radius $r = 115\ nm$. The resonant frequency $f = 674$ kHz and quality factor $Q \approx 1000$ of the nanowire were extracted from a Lorentzian fit of the vibration amplitude-frequency plot (Figure 2(b)). The tendency of having a higher Q value for thicker nanowires was observed (Figure 4(a)). The size-dependent resonance quality factor of 100-600 has previously been reported for single-clamped Ge nanowires with radii of 25-70 nm, [33] which is close to the values observed in this work for GeSn nanowires (Figure 4(a)). Such size-dependence can be explained by the increased surface-to-volume ratio for smaller radii nanowires, supporting the idea that at low pressure energy losses of such resonators are dominated by surface dissipation. [37,60]

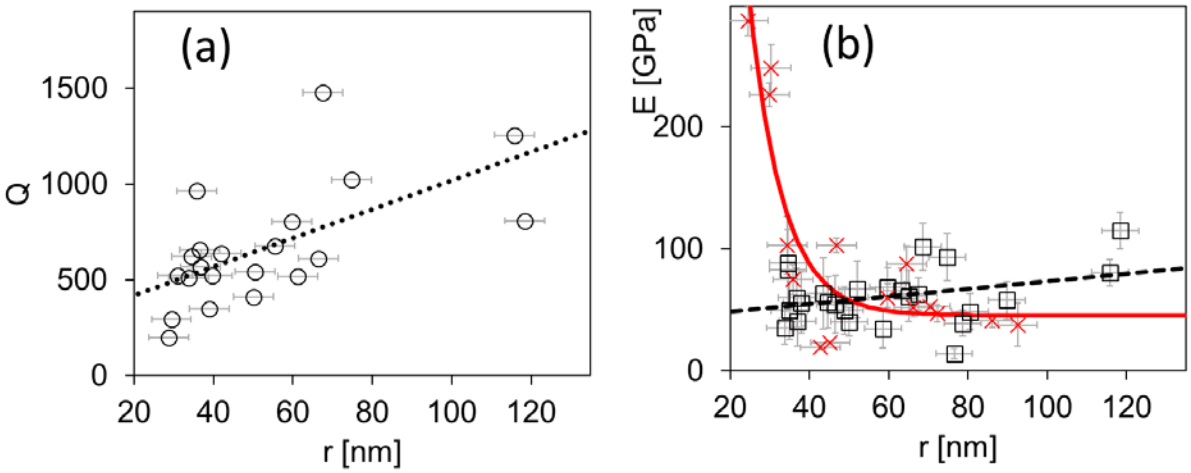

Figure 4: *(a) Experimental resonance quality factors Q vs. nanowire average radii r. Dotted black line is an empirical linear fit of experimental data (discs); (b) Experimental Young's moduli derived from resonance (squares) and 3-point bending tests (red crosses) for 41 individual GeSn nanowires vs. their average radii. Linear (dashed black line) and exponential (solid red line) extrapolation curves of the data are added as eye guidelines.*

Size-dependent Young's moduli were observed for the GeSn nanowires from the resonance and bending experiments (Figure 4(b)). From the resonance experiments, a slight increase of Young's modulus with increasing nanowire radius was observed (Figure 4(b), dashed black line), which contrasted with the experimental data from three point bending experiments of similar GeSn nanowires. An empirical exponential fit of the size-dependent bending Young's modulus (Figure 3(b), solid red line) shows an assymptotic increase at radii below 30 nm, where the highest measured Young modulus values (227-287 GPa) were twice as high as for bulk Ge (109 GPa). At radii above 30 nm, the mean Young's moduli with standard deviations extracted from the resonance (61 ± 24 GPa) and bending (59 ± 30 GPa) modes are in the same range. This is smaller than experimental Young's modulus values previously obtained for pure Ge nanowires by resonance (106 ± 19 GPa [33]) and bending (112 ± 43 GPa [28]) experiments, being closer to theoretical 82 GPa calculated for GeSn. [35]

A number of different error sources were considered to understand the accuracy of the extracted Young's moduli data. For example, measuring fundamental frequency and evaluating the boundary condition in the resonance tests, eliminating nanowire tension and sliding in the 3-point bending tests, are needed for accurate extraction of the Young's modulus from simple beam model. [39] The fundamental frequencies of the tested GeSn nanowires were measured from small amplitude linear vibrations. As the nanowires had high quality factors (Figure 4(a)), the shifts in their resonant frequencies due to damping can be assumed negligible. A fixed boundary condition was ensured by the clamp widths exceeding nanowire diameters, [54] thus enabling accurate determination of the Young's moduli from the measured experimental resonant frequencies. In the 3-point bending test, sliding of the nanowire can be a source of error. [39] This was ruled out for the measurements since there was high contact pressure at nanowire-tip interface and smooth force-displacement curves without observable hysteresis for loading-unloading (Figure 3(d)). The nanowires showed linear elastic behaviour, confirmed by AFM imaging after loading-unloading cycles. Numerical calculations performed by FEM also revealed that the strain in the nanowire during a typical mechanical bending test does not exceed 3% at displacements below 200 nm, confirming that the nanowire is in the elastic regime. The main contribution to uncertainty of the obtained values (error bars in the Figure 4(b)) was considered to be from measurements of the nanowire dimensions by SEM and AFM.

The two opposite trends of the resonance and bending Young's moduli can be explained by the influence of surface effects on the dynamic and static behaviour of the GeSn nanowires [44]. Additionally, the nanowires had different boundary conditions during resonance (fixed-free, Figure 2(b)) and three-point bending tests (fixed-fixed, Figure 3(d)), which presumes an inequal contribution of the surface on their elastic properties. [44–46] Our experimental data supports the idea that the Young's modulus, which is assumed to be an intrinsinc material

property at the macroscale, becomes very sensitive to the measurement approach at the nanoscale. [45] A theoretical model considering all effects contributing to the mechanical properties of nanowires is yet to be developed. [61] One factor which is likely to contribute to the size-dependence and reproducibility of the experimentally obtained Young's moduli for individual nanowires, would be the oxide shell (Figures 1 (c) and (d)). Previously reported Young's moduli of Ge and Sn oxides vary between ~50 GPa for Ge oxide [28,62] and 60-368 GPa for Sn oxide. [63] Amorphous oxide can have lower Young's modulus than the nanowire core due to lower density. However, the influence of a 1-2 nm thin oxide shell (Figure 1(c)) on the effective Young's modulus is expected to become noticeable only for the nanowires with radii comparable to the shell thicknesses. A simple core-shell model can be used for estimation of the composite Young's modulus if core and shell moduli and sizes are known. [38,41] An examination of the influence of an oxide shell is described in ESI. Depending on the real Young's modulus values this can lead to either stiffening or softening effect, however it is not sufficient to explain the discrepancy between the two measurement methods.

We consider that the overall size-effects in experimental Young's moduli can result from a combination of nanowire structural properties, such as bonding type, defects in crystalline structure core, presence of amorphous oxide shell, as well as the surface effects sensitive to the experimental conditions. Thus the experimental values represent effective Young's moduli, which characterise behaviours of nanomaterials at certain geometries and conditions. [45]

From our experimental results, the addition of 9 at.% Sn in Ge nanowires with radii above 30 nm causes a slight decrease the mean Young's modulus, as expected for GeSn. [35] However, this value is still comparable to other materials used in NEM devices. [32] Another important characteristics which should be considered for an active element of a NEM switch is the

ability to withstand bending deformation. Breaking strengths of 5-7 GPa were determined for the GeSn nanowires from bending experiments employing *in-situ* SEM (Figure 2(b)). These values reached 8-12 % of their Young's moduli, pre-determined for each nanowire in resonance tests. The breaking of GeSn nanowires occurred typically below 7% of strain, as was calculated from the FEM modelling, indicating, that the bending was elastic. The obtained relative breaking strength values were close to the previously reported value of ~13 % for pure Ge nanowires [28] and the theoretical limit for crystalline materials (10-16 % of E [28,50,53,64]).

Conclusions

The resonance quality factors of GeSn nanowires correlated with their radii, reaffirming the increased role of surface effects on energy dissipation in nanowire resonators. Size-dependent Young's moduli of GeSn nanowires were determined by resonance and bending methods. The differences between the experimentally determined Young's moduli obtained by the two techniques became prominent at radii below 30 nm, highlighting the importance of choosing the appropriate measurement method and consideration of boundary conditions for characterising the mechanical properties of the nanowires. The bending stresses measured at the point of fracture for the GeSn nanowires reached 8-12 % of their Young's moduli, which is comparable to the theoretical limit $E/2\pi$.

Conflicts of interest

There are no conflicts to declare.

Acknowledgements

This work was supported by the European Regional Development Fund (project No. 1.1.1.1/16/A/256, “Creation of nanoelectromechanical switches”), Science Foundation Ireland (Grant No.: 14/IA/2513) and the Irish Research Council (Grant No: GOIPG/2015/2772).

Footnotes

Electronic Supplementary Information (ESI) containing EDX analysis of GeSn nanowires and calculation example for composite Young’s modulus from core-shell model is available.

References

1 J. D. Sau and M. L. Cohen, *Physical Review B*, 2007, **75**, 45208.

2 D. W. Jenkins and J. D. Dow, *Physical Review B*, 1987, **36**, 7994.

3 A. M. Ionescu and H. Riel, *Nature*, 2011, **479**, 329.

4 C. Schulte-Braucks, S. Glass, E. Hofmann, D. Stange, N. Von Den Driesch, J. M. Hartmann, Z. Ikonic, Q. T. Zhao, D. Buca and S. Mantl, *Solid-State Electronics*, 2017, **128**, 54–59.

5 S. Wirths, R. Geiger, N. Von Den Driesch, G. Mussler, T. Stoica, S. Mantl, Z. Ikonic, M. Luysberg, S. Chiussi, J. M. Hartmann and H. Sigg, *Nature Photonics*, 2015, **9**, 88.

6 S. Al-Kabi, S. A. Ghetmiri, J. Margetis, T. Pham, Y. Zhou, W. Dou, B. Collier, R. Quinde, W. Du, A. Mosleh, J. Liu, G. Sun, R. A. Soref, J. Tolle, B. Li, M. Mortazavi, H. A. Naseem and S.-Q. Yu, *Applied Physics Letters*, 2016, **109**, 171105.

7 R. Soref, *Nature Photonics*, 2010, **4**, 495

8 S. Wirths, A. T. Tiedemann, Z. Ikonic, P. Harrison, B. Holländer, T. Stoica, G. Mussler, M. Myronov, J. M. Hartmann, D. Grützmacher, D. Buca and S. Mantl, *Applied Physics Letters*, 2013, **102**, 192103.

9 H. Wang, Y. Liu, G. Han, Y. Shao, C. Zhang, Q. Feng, J. Zhang and Y. Hao, *IEEE Transactions on Electron Devices*, 2017, **64**, 2804–2811.

10 Y.-H. Peng, H. H. Cheng, V. I. Mashanov and G.-E. Chang, *Applied Physics Letters*, 2014, **105**, 231109.

11 J. Werner, M. Oehme, M. Schmid, M. Kaschel, A. Schirmer, E. Kasper and J. Schulze, *Applied Physics Letters*, 2011, **98**, 61108.

12 P. Moontragoon, R. A. Soref and Z. Ikonic, *Journal of Applied Physics*, 2012, **112**, 73106.

13 S. Q. Yu, S. A. Ghetmiri, W. Du, J. Margetis, Y. Zhou, A. Mosleh, S. Al-Kabi, A. Nazzal, G. Sun, R. A. Soref, J. Tolle, B. Li, M. Mortazavi, H. A. Naseem and S.-Q. Yu, in *Silicon Photonics X*, 2015, vol. 9367, p. 93670R.

14 D. Stange, S. Wirths, R. Geiger, C. Schulte-Braucks, B. Marzban, N. von den Driesch, G. Mussler, T. Zabel, T. Stoica, J.-M. Hartmann and S. Mantl, *ACS Photonics*, 2016, **3**, 1279–1285.

15 M. Albani, S. Assali, M. A. Verheijen, S. Koelling, R. Bergamaschini, F. Pezzoli, E. P. A. M. Bakkers and L. Miglio, *Nanoscale*, 2018, **10**, 7250–7256.

16 X. Gong, G. Han, S. Su, R. Cheng, P. Guo, F. Bai, Y. Yang, Q. Zhou, B. Liu, K. H. Goh and G. Zhang, in *2013 Symposium on VLSI Technology*, 2013, pp. T34-T35.

17 M. Noroozi, B. Hamawandi, M. S. Toprak and H. H. Radamson, in *2014 15th International Conference on Ultimate Integration on Silicon (ULIS)*, 2014, pp. 125–128.

18 S. Gupta, R. Chen, Y.-C. Huang, Y. Kim, E. Sanchez, J. S. Harris and K. C. Saraswat, *Nano Letters*, 2013, **13**, 3783–3790.

19 C. K. Shang, V. Wang, R. Chen, S. Gupta, Y.-C. Huang, J. J. Pao, Y. Huo, E. Sanchez, Y. Kim, T. I. Kamins and others, *Applied Physics Letters*, 2016, **108**, 63110

20 A. C. Meng, C. S. Fenrich, M. R. Braun, J. P. McVittie, A. F. Marshall, J. S. Harris, P. C.-G. tx. McIntyre *Nano Letters*, 2016, **16**, 7521–7529.

21 J. Doherty, S. Biswas, D. Saladukha, Q. Ramasse, T. S. Bhattacharya, A. Singha, T. J. Ochalski and J. D. Holmes, *Journal of Materials Chemistry C*, 2018, **6**, 8738–8750.

22 M. S. Seifner, F. Biegger, A. Lugstein, J. Bernardi and S. Barth, *Chemistry of Materials*, 2015, **27**, 6125–6130.

23 S. Biswas, J. Doherty, D. Saladukha, Q. Ramasse, D. Majumdar, M. Upmanyu, A. Singha, T. Ochalski, M. A. Morris and J. D. Holmes, *Nature Communications*, 2016, **7**, 11405.

24 R. Ragan, C. C. Ahn and H. A. Atwater, *Applied Physics Letters*, 2003, **82**, 3439–3441.

25 M. S. Seifner, S. Hernandez, J. Bernardi, A. Romano-Rodriguez and S. Barth, *Chemistry of Materials*, 2017, **29**, 9802–9813.

26 S. Assali, A. Dijkstra, A. Li, S. Koelling, M. A. Verheijen, L. Gagliano, N. Von Den Driesch, D. Buca, P. M. Koenraad, J. E. M. Haverkort and E. P. Bakkers, *Nano Letters*, 2017, **17**, 1538–1544.

27 R. Meija, A. I. Livshits, J. Kosmaca, L. Jasulaneca, J. Andzane, S. Biswas, J. D. Holmes and D. Erts, *Nanotechnology*, in press, DOI: 10.1088/1361-6528/ab2b11

28 L. T. Ngo, D. Almécija, J. E. Sader, B. Daly, N. Petkov, J. D. Holmes, D. Erts and J. J. Boland, *Nano letters*, 2006, **6**, 2964–2968.

29 J. Andzane, N. Petkov, A. I. Livshits, J. J. Boland, J. D. Holmes and D. Erts, *Nano Letters*, 2009, **9**, 1824–1829.

30 J. Andzane, R. Meija, A. I. Livshits, J. Prikulis, S. Biswas, J. D. Holmes and D. Erts, *Journal of Materials Chemistry C*, 2013, **1**, 7134–7138

31 R. Meija, J. Kosmaca, L. Jasulaneca, K. Petersons, S. Biswas, J. D. Holmes and D. Erts, *Nanotechnology*, 2015, **26**, 195503.

32 L. Jasulaneca, J. Kosmaca, R. Meija, J. Andzane and D. Erts, *Beilstein Journal of Nanotechnology*, 2018, **9**, 271–300.

33 D. A. Smith, V. C. Holmberg, D. C. Lee and B. A. Korgel, *The Journal of Physical Chemistry C*, 2008, **112**, 10725–10729.

34 P. E. L. Moraes, R. J. Contieri, E. S. N. Lopes, A. Robin and R. Caram, *Materials Characterization*, 2014, **96**, 273–281.

35 X. Zhang, C. Ying, Z. Li and G. Shi, *Superlattices and Microstructures*, 2012, **52**,

459–469.

36 R. E. Miller and V. B. Shenoy, *Nanotechnology*, 2000, **11**, 139.

37 E. Pickering, A. Bo, H. Zhan, X. Liao, H. H. Tan and Y. Gu, *Nanoscale*, 2018, **10**, 2588–2595.

38 C. Q. Chen, Y. Shi, Y. S. Zhang, J. Zhu and Y. J. Yan, *Physical Review Letters*, 2006, **96**, 75505.

39 Y. Zhu, *Applied Mechanics Reviews*, 2017, **69**, 10802.

40 H. S. Park, W. Cai, H. D. Espinosa and H. Huang, *MRS Bulletin*, 2009, **34**, 178–183.

41 F. Xu, Q. Qin, A. Mishra, Y. Gu and Y. Zhu, *Nano Research*, 2010, **3**, 271–280.

42 T.-H. Chang, G. Cheng, C. Li and Y. Zhu, *Extreme Mechanics Letters*, 2016, **8**, 177–183.

43 Y. Zhu, F. Xu, Q. Qin, W. Y. Fung and W. Lu, *Nano Letters*, 2009, **9**, 3934–3939.

44 J. He and C. M. Lilley, *Applied Physics Letters*, 2008, **93**, 263108.

45 J. He and C. M. Lilley, *Nano Letters*, 2008, **8**, 1798–1802.

46 Y. Yao and S. Chen, *Mechanics of Materials*, 2016, **100**, 12–21.

47 Y. Wang, V. Schmidt, S. Senz and U. Gösele, *Nature Nanotechnology*, 2006, **1**, 186.

48 D. Wang, Y.-L. Chang, Q. Wang, J. Cao, D. B. Farmer, R. G. Gordon and H. Dai, *Journal of the American Chemical Society*, 2004, **126**, 11602–11611.

49 S. Biswas, S. Barth and J. D. Holmes, *Nano Research*, 2017, **10**, 1510–1523.

50 D. A. Smith, V. C. Holmberg and B. A. Korgel, *ACS Nano*, 2010, **4**, 2356–2362.

51 J. Kosmaca, J. Andzane, J. Prikulis, S. Biswas, J. D. Holmes and D. Erts, *Science of Advanced Materials*, 2015, **7**, 552–557.

52 J. Kosmaca, L. Jasulaneca, R. Meija, J. Andzane, M. Romanova, G. Kunakova and D. Erts, *Nanotechnology*, 2017.

53 S. Vlassov, B. Polyakov, S. Oras, M. Vahtrus, M. Antsov, A. Šutka, K. Smits, L. M. Dorogin and R. Lõhmus, *Nanotechnology*, 2016, **27**, 335701.

54 Q. Qin, F. Xu, Y. Cao, P. I. Ro and Y. Zhu, *Small*, 2012, **8**, 2571–2576.

55 C. M. Lilley and J. He, *Journal of Applied Mechanics*, 2009, **76**, 64502.

56 L. Meirovitch, *Elements of vibration analysis*, McGraw-Hill, New York, 1975

57 P. M. Morse, *Vibration and Sound*, McGraw-Hill, New York, 1948

58 W. Wang, D. Lei, Y. Dong, X. Gong, E. S. Tok and Y.-C. Yeo, *Scientific Reports*, 2017, **7**, 1835.

59 P. Periwal, T. Baron, P. Gentile, B. Salem and F. Bassani, *APL Materials*, 2014, **2**, 46105.

60 J. Bartolomé, A. Cremades and J. Piqueras, *Applied Physics Letters*, 2015, **107**, 191910.

61 A. M. Abazari, S. M. Safavi, G. Rezazadeh and L. G. Villanueva, *Sensors*, 2015, **15**, 28543–28562.

62 S. Spinner and G. W. Cleek, *Journal of Applied Physics*, 1960, **31**, 1407–1410.

63 S. Barth, C. Harnagea, S. Mathur and F. Rosei, *Nanotechnology*, 2009, **20**, 115705.

64 C. R. Barrett, W. D. Nix and A. S. Tetelman, *The principles of engineering materials*, Prentice-Hall, Englewood Cliffs, 1973.